ORNL/TM-2022/2688

Understanding FLiNaK Salt Intrusion Behavior on Nuclear- Grade Graphite via Neutron Tomography

Jisue Moon
Nidia Gallego
Cristian Contescu
James R. Keiser
Yuxuan Zhang
Erik Stringfellow

September 2022

OAK RIDGE National Laboratory

ORNL IS MANAGED BY UT-BATTELLE LLC FOR THE US DEPARTMENT OF ENERGY

ORNL/TM-2022/2688

Chemical Sciences Division

UNDERSTANDING FLINAK SALT INTRUSION BEHAVIOR ON NUCLEAR-GRADE GRAPHITE VIA NEUTRON TOMOGRAPHY

Jisue Moon
Nidia Gallego
Cristian Contescu
James R. Keiser
Yuxuan Zhang
Erik Stringfellow

September 2022

Prepared by
OAK RIDGE NATIONAL LABORATORY
Oak Ridge, TN 37831
managed by
UT-BATTELLE LLC
for the
US DEPARTMENT OF ENERGY
under contract DE-AC05-00OR22725

CONTENTS

FIGURES

TABLES

ACRONYMS

CT	computed tomography
FLiNaK	LiF-NaF-KF
HFIR	High Flux Isotope Reactor
MSR	molten salt reactor
N-CT	neutron computed tomography

ABSTRACT

Graphite is an essential material as a neutron moderator in molten salt reactors (MSRs). To understand the impact of salt on the graphite structure to develop structural materials for MSRs, molten salt intrusion behavior on nuclear-grade graphite was studied. The graphite samples, IG-110 and PCEA, were tested for infiltration with LiF-NaF-KF (FLiNaK) at 750°C, 5 bar for 12 h, and, after the intrusion experiment, the graphite was analyzed by neutron imaging. The graphite and Li from FLiNaK showed great contrast in the neutron attenuation coefficient. Thus, the salt behavior in the graphite structure has been visualized for the first time without damaging the sample. The 3D image of the graphite was reconstructed after a neutron computed tomography scan, and the average salt coverage distribution of the XY surface in different depths was obtained from the reconstructed 3D images.

1. SALT INTRUSION STUDIES

1.1 SALT INTRUSION EXPERIMENT

Setup for the salt intrusion experiments was detailed in a previously published report [1]. The high-pressure salt-infiltration rig used for the experiments consists of a graphite-lined containment vessel, which protects the salt from contact with metals, and an all-graphite sample holder which accommodates up to six graphite specimens. The sample holder is designed to allow unrestricted salt access to all vertical surfaces of graphite specimens and to most horizontal surfaces supported by the sample holder. The gas inlet and outlet located on top of the containment vessel are used to pressurize the samples from the top of the vessel. Graphite specimens were machined as 1.5 cm long parallelepiped bars with square profile (1 cm × 1 cm), and the samples were laser-marked, dried, weighed, and stored in a desiccator. Before impregnation, the graphite sample holder and the specimens were outgassed in high vacuum at 1,200°C. After mounting the specimens in the sample holder, the assembly was kept in a rough vacuum. The salt containment compartment was continually flushed with Ar while the temperature was gradually raised to melt the salt. After thermal equilibration at the targeted temperature (i.e., 750°C), the specimens were immersed in the salt, and the Ar gas pressure was raised to 5 bar (gauge pressure). After 12 h, the samples were raised above the salt level, and the system was cooled overnight while maintaining the Ar pressure. The impregnated specimens were quickly removed from the sample holder, any loose salt was brushed off, and the specimens were introduced in an Ar-filled glove box for weighing and storage in tightly closed vials.

1.2 GRAPHITE PHYSICAL PROPERTIES

The open and closed pore volumes of each graphite grade were calculated using the bulk density (ρ_{bulk}) and skeleton density ($\rho_{skeleton}$) of graphite specimens. The former was obtained from direct measurements of mass and volume, and the second was measured by helium pycnometry. The volumes of open and closed pores were calculated using the following formulae:

$$V_{open} = m\left(\frac{1}{\rho_{bulk}} - \frac{1}{\rho_{skeleton}}\right)$$

$$V_{total} = m\left(\frac{1}{\rho_{bulk}} - \frac{1}{2.24}\right),$$

where 2.24 g/cm^3 is the theoretical density of perfect graphite crystalline structure. More information on porosity distribution was obtained from mercury intrusion porosimetry. Because it does not wet graphite surfaces, mercury penetration through open graphite pores is countered by capillary forces. The relationship between the mercury pressure ΔP and the diameter d of open pores that can be penetrated at that pressure is described by the Washburn equation:

$$d = \frac{4\gamma}{\Delta P}\cos\theta\,,$$

where $\gamma = 0.484$ N/m and $\theta = 155°$ are mercury surface tension and recommended wetting angle for the mercury–graphite system [2]. Figure 1 shows the results of mercury porosimetry analysis for two types of nuclear-grade graphite, PCEA, and IG-110. The plots show the cumulative volume of mercury intruded in graphite on the increase of mercury pressure (Figure 1(a)), and the pore distribution of the two graphite samples (Figure 1(b)). IG-110 shows a sudden mercury intrusion in a narrow, well-defined pressure interval, indicating a narrow pore-size distribution. However, PCEA, which contains medium-grain graphite, shows a gradual mercury intrusion over a wide pressure interval with broadly distributed pore-size openings. Additionally, the intrusion branch shows a steeper change of slope of ~10,000 psi.

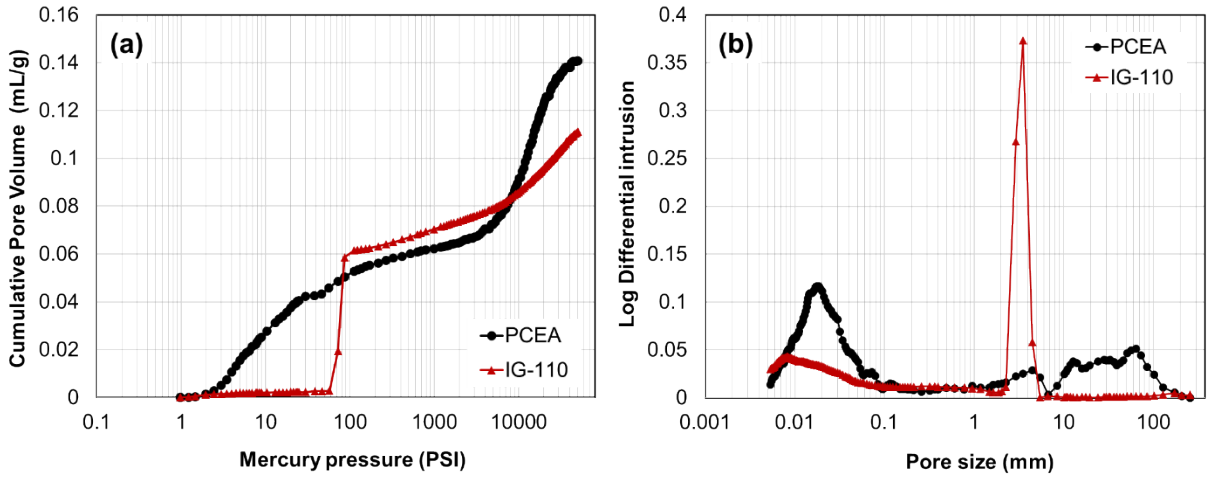

Figure 1. (a) Cumulative pore volume of mercury intrusion vs. mercury for PCEA and IG-110. (b) Log differential pore volume vs. pore size.

Table 2 lists the results of mercury porosimetry and helium pycnometry. Although they exhibit significant grain-size differences and pore diameter distributions, PCEA and IG-110 have equal porosity values (21% of apparent volume) and similar bulk density.

Table 1. Physical properties of nuclear-grade graphite tested by pore analysis method.

Graphite grade	Grain size (μm)	Bulk density (g·cm^{-3})	Open pore volume (cm^3·g^{-1})	Closed pore volume (cm^3·g^{-1})	Total pore volume (cm^3·g^{-1})	Porosity (%)	Pore diameter (μm)
PCEA	<800	1.768	0.060	0.054	0.119	20.4	10–100
IG-110	10	1.784	0.078	0.041	0.114	21.1	3.9

2. NEUTRON IMAGING STUDIES

2.1 NEUTRON IMAGING SETUP AND EXPERIMENTS

For the neutron imaging experiment, two graphite samples, including superfine (i.e., IG-110) and medium-fine (i.e., PCEA) samples, were exposed to FLiNaK at 750°C, 5 bar (i.e., gauge pressure) for 12 h. Specimen was loaded in an aluminum can with 0.6 in. diameter, and aluminum foil was positioned between the samples to separate the two graphite images during data processing. Neutron imaging tomography was done on the CG-1D beamline at the High Flux Isotope Reactor (HFIR) at Oak Ridge National Laboratory (ORNL). The CG-1D neutron imaging facility provides a polychromatic beam of a cold neutron with a peak wavelength of 2.6 Å to perform radiography and computed tomography (CT). The facility provides a collimation ratio L/D of 400, where L is the distance from the aperture of diameter D and where the radiography is formed. The beamline is equipped with Andor CCD iKon-L 936 detector. To obtain a CT image, the sample was rotated in the beam stepwise with a step size of 0.76° around a fixed axis with 0–360° coverage, allowing for the acquisition of a projection image at each rotation angle using the position-sensitive detector. The exposure time per image was 30 s. Three-dimensional images of each graphite sample were reconstructed using Amira 3D software from Thermo Scientific. The theoretical neutron attenuation coefficient of FLiNaK and graphite were calculated at with iNEUIT (iNeutron Imaging Toolbox) [3,4].

2.2 NEUTRON COMPUTED TOMOGRAPHY SCAN RESULTS FOR GRAPHITE AFTER INTRUSION EXPERIMENT

PCEA and IG-110 were exposed to the FLiNaK salt for intrusion testing at 750°C, 5 bar for 12 h. The salt-exposed graphite specimens were analyzed using neutron computed tomography (N-CT). Prior to N-CT, we attempt to analyze the graphite using x-ray imaging, but it was not successful, mainly because x-rays are predominantly sensitive to electron densities and lithium is largely invisible to x-rays. Different from x-rays, neutrons are chargeless particles and interact mainly with nuclei; therefore, neutron beam attenuation does not depend on the atomic number, while for x-rays, the high-Z elements are stronger absorbers than low-Z elements.

N-CT was used to produce a 3D real-space representation from which cross-sectional slices were extracted. Neutron attenuation radiography is based on the transmission of a collimated beam of cold neutrons through a sample and the recording of the attenuated beam by a position-sensitive detector. The transmitted intensity obeys Lambert-Beer's law, stating that for given neutron energy, the ratio of the transmitted and incident intensities is an exponential function of thickness multiplied by the attenuation coefficient of the sample.

Figure 2 shows the 3D reconstructed images of graphite samples that were exposed to the FLiNaK intrusion test. The colored map was applied based on the neutron attenuation coefficient differences over the graphite. The reconstructed image shows two distinct regions: red (~0.5 cm^{-1}) and green (~0.3 cm^{-1}). The green areas indicate a low neutron attenuation coefficient, which corresponds to graphite without salt. The red areas indicate a higher neutron attenuation coefficient, which corresponds to salts with graphite. The attenuation coefficient of the red areas is close to the summation of neutron attenuation coefficient for both graphite and salt. PCEA graphite possesses a bigger pore size, and the pores are visible on the surface of the graphite as green color due to the salt coverage on the surface difference, while IG-110 showed overall uniform salt coverage on the surface, with smaller green dots over the entire surface.

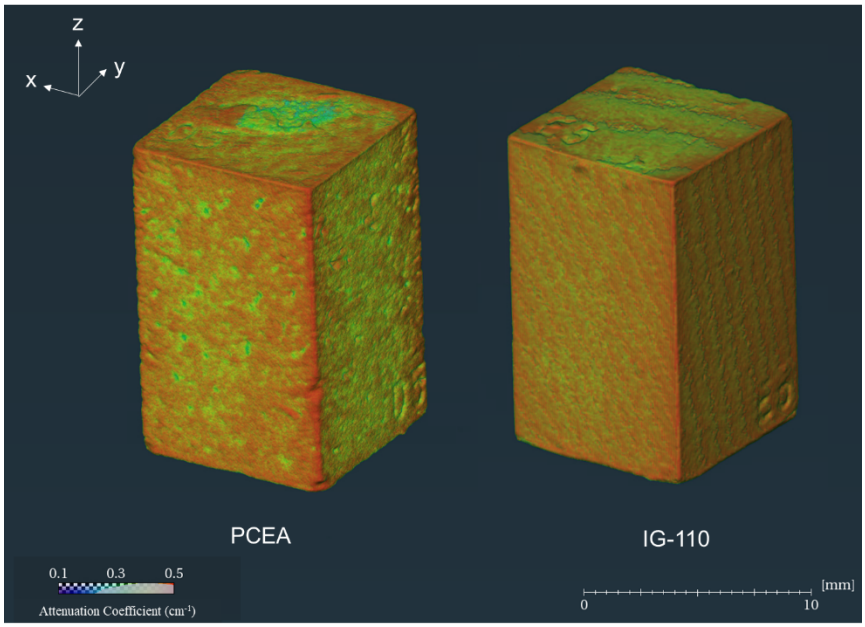

Figure 2. The 3D reconstructed images of the (left) PCEA and (right) IG-110 samples immersed in FLiNaK at 750°C, 5 bar (gauge pressure) for 12 h.

To understand the salt intrusion to the graphite structure, an XY slice image was captured with selected *z* height (Figure 3). Choosing the bottom surface, which does not have any engraving on the surface as a height of 0 (surface), the slice images were extracted with heights of 0.5, 1, 5, and 7.5 mm from the bottom of the graphite. The image at the height of 0 is not shown in the figure due to artifacts generated by graphite machining and beam hardening. A salt intrusion in the bulk graphite structure is a dominant feature. Particularly for the PCEA, which has the largest pore size (64 μm) among the nuclear-grade graphite specimens tested, salt was observed in the pores at a depth of 7.5 mm, which is about the middle of the sample height (total sample height is 15.5 mm), and salt was observed in the pores at all heights. For IG-110, which has a pore size of 3.9 μm, the middle of the graphite at the height of 7.5 mm exhibits greener than PCEA, indicating less salt in the middle of the specimen. Another interesting point is that, for both PCEA and IG-110, the surface shows an X-shaped green area, which can be explained by the introduction of gas pressure on the side of the graphite, resulting in a gradient of salt intrusion.

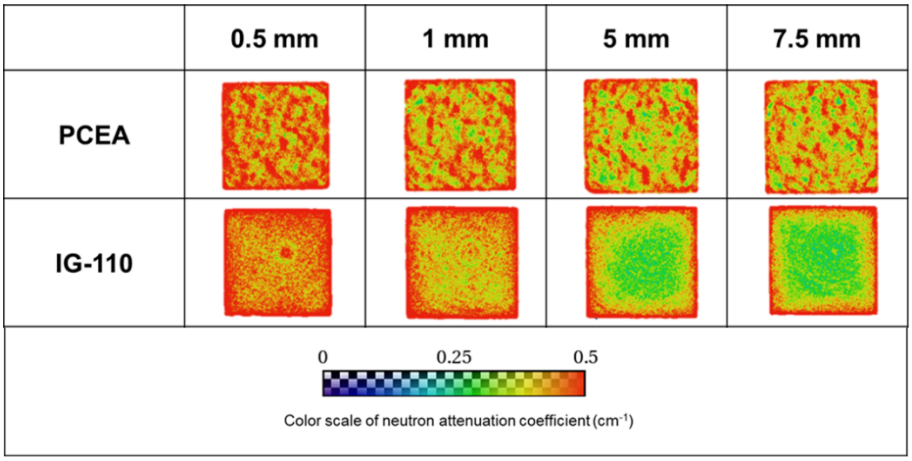

Figure 3. XY surface images with selected *z* height. The top row shows XY images of PCEA, and the bottom row shows XY images of IG-110 XY-images for heights of 0.5, 1, 5, and 7.5 mm from the bottom of the graphite. Color scale of attenuation coefficient is listed in the last row of the figure.

The salt distribution on the XY surface at the height of 7.5 mm for PCEA and IG-10 graphite samples was extracted from 3D CT scans. Figure 4 shows salt coverage over the center line at the XY surface. As can be seen in Figures 3 and 4, PCEA showed salt in the pores located in the middle of the graphite samples. Some pores located inside the graphite showed full salt coverage, and thus salt can intrude significantly in the middle of structure of the graphite. For IG-110, the salt intruded about 1.7 mm from the surface, and no significant amounts of salt were observed inside the graphite structure.

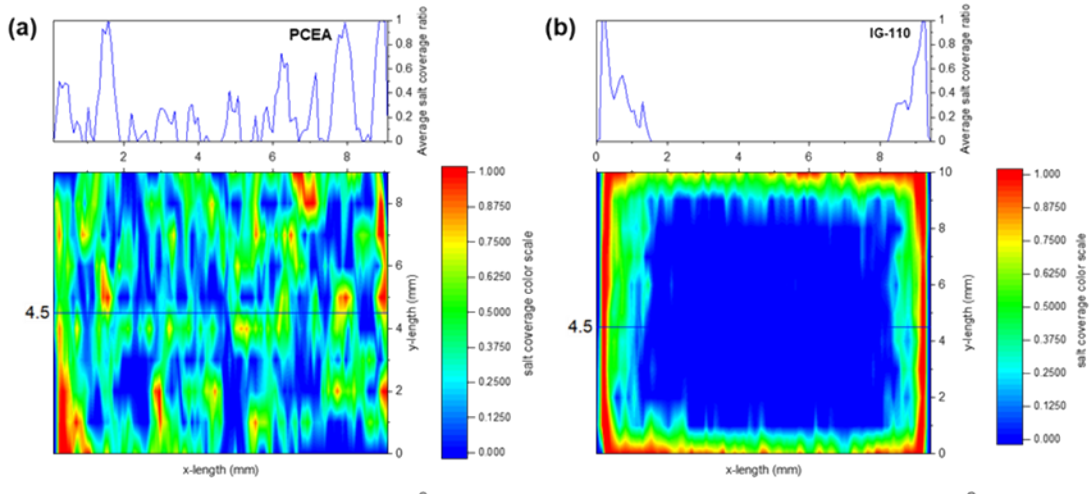

Figure 4. Salt coverage comparison between (a) PCEA and (b) IG-110, over XY surface at the height of 7.5 mm from the bottom of the graphite. Top panel shows the salt coverage over the X-axis at the 4.5 mm (Y-axis).

3. SUMMARY AND ONGOING EXPERIMENTS

This report summarizes initial neutron imaging results obtained from proof-of-principle neutron imaging experiments aimed at investigating the interaction between nuclear-grade graphite and molten salt,

FLiNaK. The results showed significant salt intrusion of the sample with the biggest pore size, proving that the pore size can significantly affect intrusion. Our results confirm that neutron imaging can be a strong, nondestructive analytical tool for understanding fluoride salt intrusion behavior over nuclear-grade graphite and thus can apply to various analytical tools before and after neutron imaging analysis.

The data analyzed for this report were obtained from proof-of-principle beamtime during the 2022A HFIR cycle. During this experiment, 3D N-CT scans of six nuclear-grade graphite specimens (i.e., PECA, IG-110, 2114, ETU-10, NBG-25, and CGB) after intrusion experiments were obtained, and the analysis of the rest of the graphite specimens (i.e., 2114, ETU-10, NBG-25, and CGB) is currently ongoing. During the proof-of-principle experiment, the fresh graphite sample image was not measured, and thus there are some discrepancies in the information regarding the fresh sample information. Currently, one general user proposal for the CG-1D beamline has been accepted and will measure the fresh sample and salt-intruded graphite sample that was exposed to different intrusion pressures in late September. To understand the intrusion effect, a second general user proposal for neutron imaging on the CG-1D beamline was submitted for 2023A cycle to study different intrusion temperatures and time effects. The successful measurement of two upcoming neutron imaging beamtimes will allow us to understand the time, temperature, and pressure effects of intrusion over nuclear-grade graphite samples exhibiting different microstructures.

4. REFERENCES

[1] N. C. Gallego, CI Contescu, and J. Keiser Progress Report on Graphite Salt Intrusion studies. ORNL Report no. ORNL/TM-2020/1621. Oak Ridge, TN: ORNL, 2020.

[2] ASTM D4284-12, “Standard Test Method for Determining Pore Volume Distribution of Catalysts by Mercury Intrusion Porosimetry,” ASTM International, 2017.

[3] Y. Zhang and J.-C. Bilheux. “ImagingReso: A Tool for Neutron Resonance Imaging.” Journal of Open Source Software 2(19) (2017): 407.

[4] Y. Zhang, J.-C. Bilheux, H.Z. Bilheux, and J.Y. Lin. “An Interactive Web-Based Tool to Guide the Preparation of Neutron Imaging Experiments at Oak Ridge National Laboratory.” *Journal of Physics Communications* 3(10) (2019): 103003.